Direct Detection of Near-surface Faults by Migration of Back-scattered Surface Waves

Han Yu[1], Bowen Guo[1], Sherif Hanafy[1], Fan-Chi Lin[2], and Gerard T. Schuster[1]
1 Physical Sciences and Engineering, King Abdullah University of Science and Technology, Thuwal 23955-6900
2 Department of Geology and Geophysics, University of Utah, Salt Lake City, UT 84112

SUMMARY

We show that diffraction stack migration can be used to estimate the distribution of near-surface faults. The assumption is that near-surface faults generate detectable back-scattered surface waves from impinging surface waves. The processing steps are to isolate the back-scattered surface waves, and then migrate them by diffraction migration using the surface wave velocity as the migration velocity. Instead of summing events along trial quasi-hyperbolas, surface wave migration sums events along trial quasi-linear trajectories that correspond to the moveout of back-scattered surface waves. A deconvolution filter derived from the data can be used to collapse a dispersive arrival into a non-dispersive event. Results with synthetic data and field records validate the feasibility of this method. Applying this method to USArray data or passively recorded exploration data might open new opportunities in mapping tectonic features over the extent of the array.

INTRODUCTION

Engineering and exploration surveys are used to detect the distribution of near-surface faults. Accurate fault maps can be used to avoid unsafe construction of buildings or placement of drilling platforms. Detection of hidden faults near the surface can also be used to predict the optimal location of paleoseismic trench surveys that determine the magnitude and recurrence intervals of ancient earthquakes.

Shallow seismic surveys *indirectly* detect the presence of near-surface faults by computing reflection sections, and inferring faults from the discontinuities of the reflection horizons. This indirect procedure is often successful, but it requires careful processing of the data to extract the reflection events, estimation of the correct stacking velocity, and sometimes a rigorous estimate of the statics. Moreover, the very early arrivals are muted due to the limitations in source-receiver sampling, so the reflectors very close to the surface are ignored. Such ignorance might prevent the detection of faults within several wavelengths of the free surface. For interferometric processing of passive seismic data, body-wave reflections are very difficult to extract, especially from shallow layers.

This paper proposes the *direct* detection of near-surface faults by diffraction migration of back-scattered surface waves. The faults are *directly* detected by migrating the back-scattered surface waves to their place of origin along the fault. The key assumption is that near-surface faults generate detectable back-scattered surface waves from impinging surface waves. This migration procedure is related to the interferometry method proposed by Schuster et al. (2012) except the data are directly migrated, rather than interferometrically redatumed, for trial

image points on the surface. The processing steps are to isolate the back-scattered surface wave events, and then migrate them by diffraction migration using the surface wave velocity as the migration velocity. Instead of summing events along trial hyperbolas, surface wave migration sums events along trial quasi-linear trajectories that correspond to that of the back-scattered surface waves. A deconvolution filter derived from the data can be used to collapse the dispersed surface wave arrival into a non-dispersive event. Results with synthetic data and field records validate the feasibility of this method.

The first part of this paper presents the theory, the second part shows numerical results with both synthetic data and field data. The field data are for a seismic survey over a desert region with faults at the near surface. The final section presents conclusions.

THEORY OF SURFACE WAVE MIGRATION

The vertical-component particle velocity of a propagating Rayleigh wave over a homogeneous half space can be approximated by the harmonic Green's function

$$G(\mathbf{g}|\mathbf{s}) = W(\omega)A(\mathbf{g},\mathbf{s})e^{ik|\mathbf{g}-\mathbf{s}|}e^{-\kappa|z|}, \qquad (1)$$

where the source at $\mathbf{s}$ and vertical-component particle-velocity geophone at $\mathbf{g}$ are both on the free surface (Aki and Richards, 1981), and κ is the vertical component of the wavenumber vector. The horizontal wavenumber is given by $k = \omega/c$, where c is the Rayleigh wave velocity in a homogeneous medium for Figure 1 and ω is the angular frequency of the vertical component point source on the free surface. The term $A(\mathbf{g},\mathbf{s})$ takes account into the geometrical spreading of the surface wave and $W(\omega)$ is the source wavelet spectrum that also includes a phase term associated with the Green's function for the surface wave; for convenience we will assume that this phase term is deconvolved from the data.

As an example, Figure 1 shows the simulated surface waves for a model with three homogeneous blocks of velocity. The back-scattered surface waves are the events that moveout in the opposite direction of the incident surface wave. These records are computed by a finite-difference solution to the 2D elastic wave equation.

Previous work (Snieder, 1986; Blonk and Herman, 1994; Campman et al., 2003; van Wijk, 2003) on imaging Rayleigh wave scattering from impedance discontinuities approximates the scattered waves at the free surface as a weighted surface integral of Green's tensors that take into account surface-wave propagation. The weights are impedance discontinuities $\sigma(\mathbf{x})$ on the free surface or very near the free surface and the integration is over the free surface; the impedance discontinuity can be considered to be a function of frequency to account
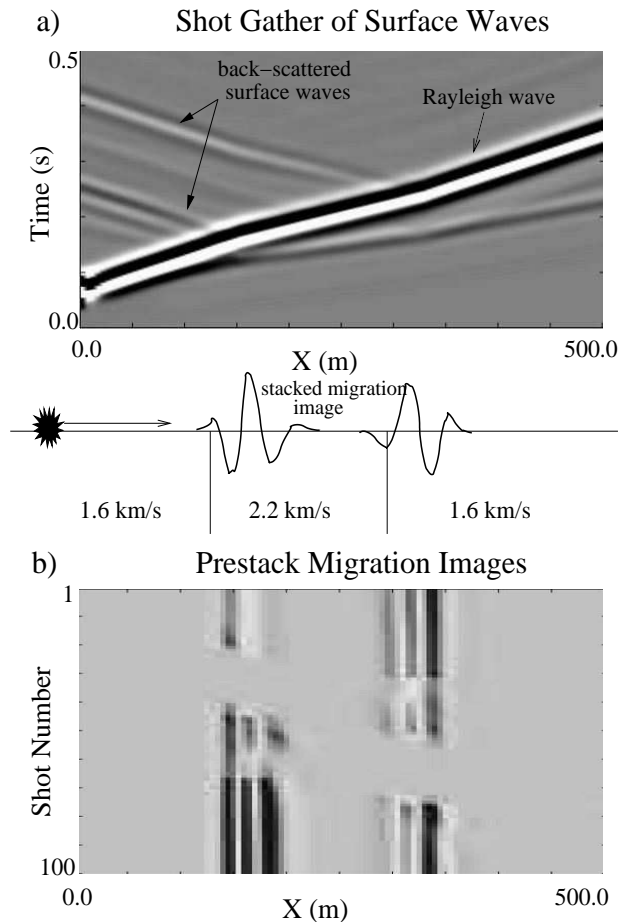
Figure 1: a) Simulated surface wave records for a vertical-displacement point source (star) at $\mathbf{s} = (x_s, 0)$ and vertical component geophones on the free surface. The vertical lines in the middle are the faults that separate one velocity block from another. The velocities depict those of the simulated Rayleigh wave. b) Prestack migration images obtained by migrating the back scattered Rayleigh waves in 100 shot gathers. The stacked migration image is given by the solid line along the surface of the fault model.

for depth variations in the impedance function. The inverse to this integral equation gives the impedance distribution. In our proposal, we simply assume that the surface-wave response to an impedance discontinuity represented by a near-surface fault can be approximated by a surface integral of Green's functions weighted by the impedance discontinuity associated with the fault. Instead of inverting this equation in the least squares sense, we will simply apply its adjoint to the data to get the migration image on the surface.

The following steps are used to migrate the back-scattered surface waves to their point of origin along the fault near the surface. The key assumption is that the dominant back-scattered arrivals are from the near-surface portions of the fault.

1. We will assume that the traveltime of surface waves from

$\mathbf{x}$ to $\mathbf{x}'$ at a specific frequency is given by $\tau_{xx'}$, where the traveltime dependence on frequency is silent. If the subsurface is homogeneous then the velocity is independent of frequency, but if the Rayleigh wave is dispersive then we can perform migration in the frequency domain using the phase velocity as the migration velocity. Alternatively, we can assume that the dispersive wavelet has been compressed to a narrow wavelet using a suitable deconvolution filter[*]. In this case the forward data can be approximated by equation 1 and the back-scattered surface waves $\tilde{d}(\mathbf{x}|\mathbf{s})^{scatt}$ can be approximated by

$$\tilde{d}(\mathbf{g}|\mathbf{s})^{scatt} = W(\omega)A(\mathbf{s},\mathbf{x}_o)A(\mathbf{g},\mathbf{x}_o)re^{i\omega(\tau_{sx_o}+\tau_{gx_o})}, \; x_g, x_s < x_o, \; (2)$$

where the back-scattered reflection coefficient is denoted by r, the vertical fault is to the right of the source at $\mathbf{x}_o = (x_o, 0)$, and the back-scattered field at $\mathbf{g} = (x_g, 0)$ is only alive to the left of the fault. Here, $A(\mathbf{g}, \mathbf{x}_o)$ accounts for geometrical spreading from the scatterer location at $\mathbf{x}_o$ to $\mathbf{g}$ at the left of the fault.

2. The back-scattered data are migrated $\tilde{d}(\mathbf{g}|\mathbf{s})^{scatt}$ ($x_g, x_s < x_o$) using the diffraction stack migration formula

$$m(\mathbf{x}') = \sum_g \tilde{d}(\mathbf{g}|\mathbf{s})^{scatt} e^{-i\omega(\tau_{sx'}+\tau_{gx'})} \mathscr{W}(\omega)^{-1}, \; x_g, x_s < x', \quad (3)$$

where $m(\mathbf{x}')$ is the migration image at the trial image point $\mathbf{x}' = (x', 0)$ such that $x_g < x'$ and $\mathscr{W}(\omega)^{-1}$ is the deconvolution filter that also accounts for dispersion effects.

3. Plugging equation 2 into equation 3 gives

$$m(\mathbf{x}') = \sum_g A(\mathbf{g},\mathbf{x}_o)A(\mathbf{s},\mathbf{x}_o)re^{-i\omega(\tau_{sx'}+\tau_{gx'}-\tau_{sx_o}-\tau_{gx_o})}. \quad (4)$$

with $x_g, x_s < x'$. If $x' = x_o$ then the migration formula becomes

$$m(\mathbf{x}') = \sum_g A(\mathbf{g},\mathbf{x}_o)A(\mathbf{s},\mathbf{x}_o)r, \; x_g, x_s < x'. \quad (5)$$

which coherently sums over all frequencies. This formula provides the maximum amplitude in the migration image on the surface, and therefore pinpoints the location of the fault. If the fault does not break the free surface, then we can assume that the interaction of the surface wave with the near-surface fault generates a body wave that propagates from the buried fault to the surface, and transforms into a back-scattered surface wave. This extra time delay from the subsurface fault plane to the surface can be accounted for by an extra phase term $e^{-i\omega\tau_{x'g}}$ in the migration kernel[†], which can be ignored if the fault is less than a quarter of a wavelength from the free surface. If the time delay cannot be ignored then the trial image points should also be just below the free surface and the extra phase term should be incorporated into the migration operator.

4. The space-time version of the migration equation can be obtained by summing equation 3 over all frequencies to give

$$
\begin{aligned}
m(\mathbf{x}') &= \sum_{\omega} \sum_{g} \tilde{d}(\mathbf{g}|\mathbf{s})^{scatt} e^{-i\omega(\tau_{sx'}+\tau_{gx'})} \mathscr{W}(\omega)^{-1}, \\
&= \sum_{t} \sum_{g} d(\mathbf{g}, \tau_{sx'}+\tau_{gx'}|\mathbf{s},0)^{scatt}, \quad (6)
\end{aligned}
$$

where $d(\mathbf{g}, \tau_{sx'}+\tau_{gx'}|\mathbf{s},0)$ is the deconvolved backscattered surface-wave data in the space-time domain at the listening time denoted by $\tau_{sx'}+\tau_{gx'}$. This listening time is physically interpreted as the quasi-linear moveout of the dominant portion of the back-scattered surface wave. In fact, it moves out with the group velocity if the dispersion effects have been properly deconvolved. Alternatively, the data can be migrated in the frequency domain at the phase velocity of the surface wave. The summation over the horizontal geophone coordinates says that the migration image is obtained by summing the back-scattered surface-wave data over trial quasi-linear curves in $x_g - t$ space associated with the trial image point at $\mathbf{x}' = (x',0)$. This compares to reflection migration which sums the reflection data over trial quasi-hyperbola curves associated with the trial image point at $\mathbf{x}'$.

5. However, caution is needed for interpretation because a fault, a topography variation, or a near-surface impedance anomaly can all generate backscattered surface waves. To alleviate this interpretation ambiguity, back-scattered surface waves in 3D data should be migrated so that long linear features in the migration image are likely to indicate linear faults, not isolated impedance anomalies.

NUMERICAL RESULTS

A 2D staggered-grid finite-difference elastic method (Virieux, 1986) is used to compute 100 shot gathers for the sources on the surface in the Figure 1a model. The data were filtered to only give the backscattered arrivals, and the filtered traces were migrated by equation 3 to give the prestack migration images depicted in Figure 1b; stacking these prestack images gives the stacked migration image depicted by the thick solid line (see middle portion of figure). The location of the two faults are clearly delimited in the migration images.

A total of 120 shot gathers were recorded near the Gulf of Aqaba in Saudi Arabia, where each shot gather contained 120 traces and the source and the receiver sampling intervals are both 2.5 m. First arrivals were picked and inverted to give the velocity tomogram in Figure 2d. It shows the location of the visible fault that break the surface at the position 2 and just beneath the surface at 1. A typical shot gather is shown in Figure 2a and the common offset gather (COG) at the source-receiver offset of 0 m is shown in Figure 2d; the COG has two distinct breaks in the reflector at the locations of the faults 1 and 2 in the tomogram. Shot gathers of backscattered arrivals are FK filtered to isolate the backscattered events shown in Figures 2b. The backscattered events are migrated for all 120 shot gathers according to equation 3 to give the prestack

migration images in Figure 2c and the stacked migration image. These migration images indicate that faults are present at offset locations of 150 and 250 m. These interpreted fault locations agree with those indicated in the first-arrival travel-time tomogram and zero-offset COG in Figure 2d. The fault at $X = 150\,m$ is observed at the surface.

CONCLUSIONS

We show that diffraction stack migration can be used to *directly* map the distribution of near-surface faults. Unlike the indirect method of detecting discontinuous reflectors in a stacked reflection section, the direct method simply isolates the backscattered surface waves and migrates them to their place of origin along the fault plane. The assumption is that near-surface faults generate detectable back-scattered surface waves from impinging surface waves. Instead of summing events along trial hyperbolas, surface wave migration sums events along trial quasi-linear trajectories that correspond to the one-sided moveout of back-scattered surface waves. A deconvolution filter derived from the data can be used to collapse a dispersive arrival into a non-dispersive event. Results with synthetic data and field records validate the feasibility of this method.

We now can migrate back-scattered surface waves, one of the strongest signals in a shot record, to directly detect the presence of faults that are just below the surface or hidden by foilage. Applying this method to USArray data or passive exploration data that have been interferometrically processed might open new opportunities in mapping tectonic features over the extent of the array. This is especially true with passive seismic data where it is very easy to generate virtual surface waves but very difficult to generate virtual reflections.

ACKNOWLEDGMENTS

a). Common Shot Gather #20

c). Prestack Migration Images

Stacked Migration Image

b). F-K Filtered Shot Gather #20
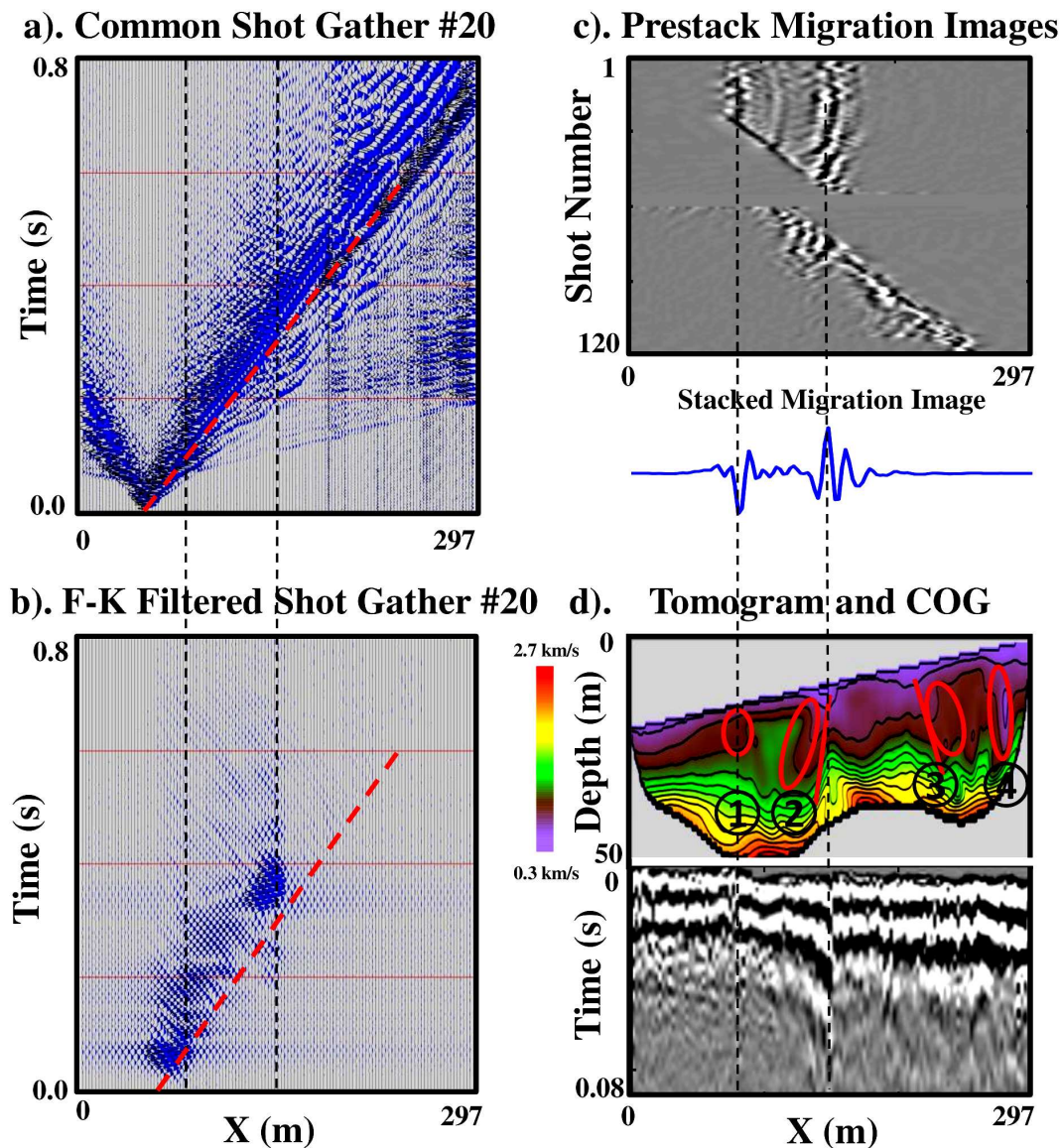
d). Tomogram and COG

Figure 2: a) Common shot gather #20, b) FK filtered shot gather, c) prestack migration images of backscattered surface waves, d) tomogram (① unidentified anomaly; ② colluvial wedge and the 1995 fault; ③ a possible fault and colluvial wedge; ④ a possible colluvial wedge), and zero-offset COG computed from the Aqaba seismic data. The stacked migration image indicates two fault locations that are consistent with those in the tomogram and COG.

http://dx.doi.org/10.1190/segam2014-0737.1

EDITED REFERENCES
Note: This reference list is a copy-edited version of the reference list submitted by the author. Reference lists for the 2014 SEG Technical Program Expanded Abstracts have been copy edited so that references provided with the online metadata for each paper will achieve a high degree of linking to cited sources that appear on the Web.

REFERENCES

Aki, K., and P. Richards, 1980, Quantitative seismology: W. H. Freeman & Company.

Blonk, B., and G. C. Herman, 1994, Inverse scattering of surface waves: A new look at surface consistency: Geophysics, **59**, 963–972, http://dx.doi.org/10.1190/1.1443656.

Campman, X. H., K. Wijk, J. A. Scales, and G. C. Herman, 2003, Suppression of near-field scattered surface waves: 65th Conference & Exhibition, EAGE, Extended Abstracts, P078.

Schuster, G. T., S. Hanafy, and Y. Huang, 2012, Theory and feasibility tests for a seismic scanning tunneling macroscope: Geophysical Journal International, **190**, no. 3, 1593–1606, http://dx.doi.org/10.1111/j.1365-246X.2012.05564.x.

Snieder, R. K., 1986, 3D Linearized scattering of surface waves and a formalism for surface wave holography: Geophysical Journal of the Royal Astronomical Society, **84**, 581–605.

van Wijk, K., 2002, Multiple scattering of surface waves: Ph.D. dissertation, Colorado School of Mines.

Virieux, J., 1986, P-SV wave propagation in heterogeneous media: Velocity-stress finite-difference method: Geophysics, **51**, 889–901, http://dx.doi.org/10.1190/1.1442147.